Combined Scanning Tunneling Microscopy and Infrared Spectroscopic Characterization of Mixed Surface Assemblies of Linear Conjugated Guest Molecules in Host Alkanethiolate Monolayers on Gold

T. D. Dunbar,[†,§] M. T. Cygan,[†] L. A. Bumm,[†] G. S. McCarty,[†] T. P. Burgin,[‖] W. A. Reinerth,[‡] L. Jones, II,[‡] J. J. Jackiw,[†] J. M. Tour,*,[‡,⊥] P. S. Weiss,*,[†] and D. L. Allara*,[†]

Department of Chemistry, Pennsylvania State University, University Park, Pennsylvania 16802-6300, and Department of Chemistry and Biochemistry, University of South Carolina, Columbia, South Carolina 29208

Received: October 19, 1999; In Final Form: March 1, 2000

Molecular resolution scanning tunneling microscopy (STM) imaging and high sensitivity infrared reflection spectroscopy (IRS) measurements have been combined to characterize the structures of mixed self-assembled monolayers (SAMs) of fully conjugated, linear thiolate-terminated molecules and short chain (8−12) *n*-alkanethiolates on Au{111}. Immersion of preformed, ordered alkanethiolate SAMs into dilute solutions of the conjugated molecules results in two-dimensional matrix isolation of conjugated adsorbates in the host SAM. The post-immersion host SAM matrix shows retained alkanethiolate ordering with the guest molecules inserted both singly into boundaries between SAM structural domains and in bundles at substrate step edges. Inserted molecules of lengths in the ~15 Å range adopt surface orientations similar to those of alkanethiolate molecules at all compositions, including the pure conjugated SAMs. In contrast, the configuration of an inserted, long conjugated molecule (~40 Å), varies monotonically with the final SAM composition. When inserted at decreasing fractions into an *n*-octanethiolate matrix, the average tilt of the long molecular axis decreases and approaches alignment with the host SAM. Combined quantum chemical calculations and IRS data for the short guest−host SAMs support a picture of a dense local environment of the host SAM around the guest molecules, despite their insertion at host defects. These results have important implications for designing electronic devices based on the addressing of individual, fully conjugated molecules self-assembled at gold electrodes.

I. Introduction

There is significant interest in learning how to design and construct nanometer-scale devices based on molecular assemblies, e.g., nanometer-scale mechanical switches,[1] an artificial blood cell with nanometer-scale pumps,[2] or electronic circuits with individual molecules as their active components.[3] While the variety and complexity of such devices is significant, some common issues exist. For devices in which electronically active molecules (EAMs) are electrically addressed, either individually or in groups, the issue of how to achieve a desired distribution and alignment of the molecules at the electrode must be considered, regardless of the exact function of the device.[4] Further, the rational design of such devices will require an extensive database of molecular electronic conductivities. The efficiency of obtaining accurate experimental data for this purpose revolves around the issue of how to configure molecules precisely at controlled electrical contacts.

Toward this end, we recently reported different methods for isolating fully conjugated linear molecules with terminal sulfur groups in alkanethiolate self-assembled monolayers (SAMs) at gold surfaces.[5] The results demonstrate that coassembly from binary solutions of $C_{12}H_{25}SH$ and any of the fully conjugated

molecules listed in Table 1 results in poorly organized films, as shown by scanning tunneling microscope (STM) images and infrared spectroscopy (IRS). In contrast, insertion of the molecules into a preassembled dodecanethiolate SAM via solution exchange results in well-organized film structures with the inserted molecules located at defect regions in the alkanethiolate host matrix. The STM images further suggest that the isolated conjugated molecules exhibit significantly higher conductivities than that of surrounding alkanethiolate lattice molecules.[5,6] These results show a way of isolating large EAMs in an "insulating" lattice and suggest qualitatively that the inserted molecules are oriented outward on the electrode surface, similar to the alkanethiolate chains.

One of the ultimate goals of our studies is to characterize in accurate detail the electronic characteristics of individual molecules bound at electrode surfaces. Since STM reports an image that is a convolution of the geometric and electronic nature of a surface,[7] in order to extract fundamental data from the images it is necessary to define first the specific adsorbate orientations and local environments by independent means. In our first report,[5] the latter characteristics were not controlled nor addressed in a quantitative way. In a recent study of mixed alkanethiolate lattices containing only alkyl chains of different lengths, we have been able to control precisely the geometry of adjacent molecules of different lengths by maintaining the basic superlattice structure.[8] In this case, the common steric character of all fully extended alkyl chains allows the translational symmetry to remain unbroken across domains of different
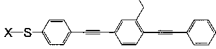

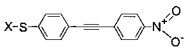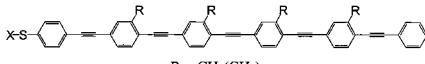Spectroscopic Characterization of Mixed Surface Assemblies

J. Phys. Chem. B, Vol. 104, No. 20, 2000 **4881**

TABLE 1: Summary of the Notations, Chemical Structures and Lengths of Fully Conjugated Molecules Referred to in the Text[a]

Notation	Chemical Structure	~Length, Å
1: X = · 1a: X = H 1b: X = Ac	X–S—	19.5
2: X = · 2a: X = H 2b: X = Ac	X–S—	13.5
3: X = · 3a: X = H 3b: X = Ac	X–S— R = CH₃(CH₂)₁₁	40.2

[a] The lengths are determined from molecular models and are defined as the distance from the S atom to the opposite terminal atom (H or O).

length molecules and this has allowed us to measure the relative conductances of adjacent molecules of different lengths.[9] In contrast, the present case consists of films with quite dissimilar adsorbate molecules formed from insertion of large aromatic thiol molecules at irregularly spaced defect sites in short alkanethiolate SAMs. In this case, determination of the average molecular configuration cannot be inferred but, rather, requires deduction from spectroscopic probes.

In this report, we describe the results of our studies to combine high sensitivity, quantitative infrared spectroscopy with molecular resolution STM in order to develop a detailed picture of the molecular configurations of inserted, linear fully conjugated molecules in alkanethiolate SAMs on Au{111} surfaces. While molecule **1** was the focus of the first study,[10] for this second study we focused instead on molecules **2** and **3** (Table 1). The latter provide extremes of molecular lengths (refer to Table 1) so that when inserted they can protrude well beyond or be immersed completely within the host alkanethiolate matrices. Molecule **2**, which includes a nitro substituent, was of interest since the strong, characteristic NO₂ vibrational modes serve as useful probes for molecular orientation and local chemical environments. Further, the presence of this group provides an example of an electronically asymmetric structure that has recently been incorporated into a fully conjugated molecule capable of functioning as a resonant tunneling diode.[11] Of particular interest are the issues of how the insertion kinetics, orientations, and electronic responses of the guest molecules depend on the host SAM thickness. Accordingly, in contrast to our first study that focused on the $C_{12}H_{25}S-$ SAM, in the present study a series of alkanethiolate SAMs ranging from $C_8H_{17}S-$ to $C_{14}H_{29}S-$ was used. Longer alkanethiolates were not used since obtaining molecular resolution STM images with these thicker films is difficult with present state-of-the-art STM instrumentation.

This paper is organized as follows. We first determine the approximate orientation of **2** to be near that of alkanethiolates on gold. Then we show that the orientation of **2** inserted into an alkanethiolate on gold matrix is exactly the same as that for a full monolayer of **2**, and consequently, similar to that of the alkanethiolate matrix. Using IRS-determined peak positions of the nitro group in conjunction with density functional theory (DFT) calculations, we show that the environment of the nitro group changes depending upon the length of the alkanethiolate matrix. We apply this information to a qualitative interpretation of the STM-observed height differences between **2** and the alkanethiolate host matrix. Finally we show that the orientation

of **3** inserted into an octanethiolate matrix depends on the monolayer composition.

2. Experimental Section

2.1 Sample Preparation. Procedures for synthesis of compounds **2b** and **3b** are reported elsewhere.[5,12] Since the parent thiols are susceptible to air oxidation, the more stable thioacetyl derivatives were synthesized. The corresponding thiols used to form the SAMs are generated in situ by hydrolysis with added base; the standard conditions were 6 μL of 30% NaOH per mg of thioacetyl derivative.[13]

The alkanethiols: octanethiol, decanethiol, dodecanethiol, and tetradecanethiol ($C_nH_{2n+1}SH$, $n = 8, 10, 12, 14$), were obtained commercially (Aldrich) and further purified by standard vacuum distillation procedures. The final purities were checked by ¹H NMR and mass spectral analyses. Hexane and acetone (Aldrich; HPLC grade) and ethanol (Pharmco; USP grade) solvents were used directly from freshly opened containers. Tetrahydrofuran (Aldrich) was freshly purified before each use by distillation over a metallic sodium and benzophenone mixture under a N₂ atmosphere.

In general, the sample preparation and handling procedures are the same as reported in our earlier study.[5] For convenience, important details are briefly presented here. Two types of gold substrates were used: Au/mica for STM and Au/Cr/SiO₂/Si for IRS.[14] Previous work has established that, despite the morphological differences between single crystal Au(111) substrates and smooth, {111} textured polycrystalline Au substrates, the structures of the associated alkanethiolate SAMs are highly similar,[14] allowing valid comparisons. The freshly evaporated Au/Cr/SiO₂/Si samples were immediately characterized using single wavelength ellipsometry and then used within 20 min ambient exposure to form the SAMs by a two-stage deposition process. Formation of alkanethiolate on gold monolayers was carried out on the benchtop under ambient conditions. Both full monolayer self-assemblies of and insertions of conjugated oligomers were carried out completely under an anaerobic atmosphere of N₂ in a sealed box. The Au/mica films were similarly handled but no ellipsometry was done. All monolayer preparations were carried out at 25 ± 2 °C. Pure alkanethiolate SAMs were prepared by an 18 h or longer immersion in a 1 mM ethanol solution containing the alkanethiol. The samples were withdrawn, rinsed in hexane, acetone, and ethanol, and blown dry under an inert atmosphere and finally stored under dry nitrogen. In cases of the Au/Cr/SiO₂/Si substrates, the samples were characterized by ellipsometry and IRS and then returned to the anerobic chamber. For convenience, the alkanethiolate SAMs formed from octanethiol, decanethiol, dodecanethiol, and tetradecanethiol are referred to as **A8**, **A10**, **A12**, and **A14**, respectively. The pure SAMs of the conjugated molecules were formed by immersion of the gold substrates in dilute O₂-free THF solutions containing the thioacetyl derivatives and base. The samples were removed and thoroughly washed sequentially in THF, acetone, and ethanol. Insertion of the aromatic molecules was carried out by immersion of the alkanethiolate SAMs into O₂-free, base-containing THF solutions of the thioacetyl derivative of the selected molecule. Experiments were carried out using arylthioacetyl concentrations ranging from 0.01 to 0.3 mM (with the addition of 6 μL of NH₄OH (30%) per mg of arylthioacetyl) and immersion times ranging from minutes to hours, respectively. After the immersion period, the samples were removed and treated as for the pure aromatic SAMs. All samples were stored under N₂ or Ar prior to analysis.
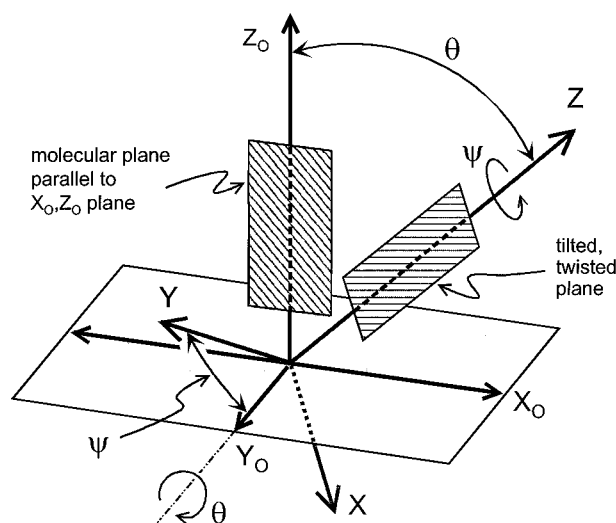
Figure 1. Coordinate diagram defining the tilt and twist angles (θ,ψ) of the aromatic ring plane from the surface normal. The Z-axis is parallel to the long molecular axis.

2.2 Single Wavelength Ellipsometry, Infrared Spectroscopy and Scanning Tunneling Microscopy. Details of the single wavelength ellipsometry (SWE), infrared spectroscopy (IRS), and scanning tunneling microscope (STM) instruments and procedures have been reported previously.[5]

The SWE measurements were used to deduce film thicknesses using established modeling methods[15−17] in conjunction with the complex refractive index expressed as a scalar, $\hat{n} = n + ik$, for isotropic films, or a tensor ($\hat{n}_{ij}$), for anisotropic films.[18] For all compounds in this study, k (or k_{ij}) = 0 at 632.8 nm, the SWE wavelength. A value of $n = 1.50$ was used for alkanethiolate films.[17] Estimates of $n = 1.64$ and 1.50 for **2a** and **3a**, respectively, were made by an atom-fragment quantitative structure−activity relationship (QSAR) method developed by Ghose and Crippen.[19] The required densities for these estimates were measured by the crystal-float method to give values of $1.28(\pm 0.02)$ and $0.90(\pm 0.02)$ g cm^{-3}, respectively, for derivatives **2b** and **3b**. These values agreed, within the errors of the methods, with those determined by an atom-fragment density estimation method.[20] All the refractive index and density values of the derivatives were assumed to apply to the surface species **2** and **3**. An effective medium approximation was applied to estimate the refractive index of heterogeneous films.[21]

The IRS spectra were used to deduce the average surface densities and orientations of adsorbed conjugated molecules. The primary approach involved previously described simulation methods,[22] but more approximate band intensity ratioing methods were used as well.[23] The orientations are defined in terms of the tilt angles of the long molecular axis and the twist of the aromatic plane, assuming a completely planar conjugated molecule. A coordinate diagram is given in Figure 1. The optical function (complex refractive index) spectra of the bulk solid phases of the molecules were obtained using dispersions of the molecules at measured compositions in pressed KBr disks.[22] Anisotropic optical function tensor spectra were generated by assigning each component peak in the isotropic optical function spectra to a specific vibrational mode and then constructing the tensor for a given molecular orientation according to the direction of the transition dipole moment of each mode.[22] Summaries of the modes are given in Tables 2 and 3. For treatment of heterogeneous media, the effective medium approximation was applied.[21] For quantitative analysis of spectra of **2** inserted into the alkanethiolate matrices, the following mode

peaks were chosen because of their spectral contrast and well-defined transition dipole moment directions: 1344 cm^{-1} [NO$_2$ symmetric stretch, ν_{sym} NO$_2$], 1530 cm^{-1} [antisymmetric NO$_2$ stretch, ν_{asym} NO$_2$], 2212 cm^{-1} [C≡C stretch, $\nu_{C≡C}$], 866 cm^{-1} [out-of-plane ring mode, ν_{17b}], and 1597 cm^{-1} [C=C tangential ring stretching, ν_{8b}]. The fractional insertion of **3** inserted into alkanethiolate matrices was followed by SWE and by the diagnostic modes: 1504 cm^{-1} [C=C ring stretching, ν_{19a}], 1595 cm^{-1} [C=C ring stretching, ν_{8a}], $\sim$830 cm^{-1} [out-of-plane ring mode, ν_{10a}], and 754 cm^{-1} [out-of-plane ring mode, ν_{11}]. In each case, modes assigned to the thioacetyl group were not analyzed since this group is not incorporated in the final SAMs.[24]

All STM images were taken in the conventional constant dc current mode[5] in an inert gas purged chamber.[25] All the samples studied were sufficiently conductive that the large tunneling gap impedances ($\geq 10^{11}$ Ω) used could maintain the tip position above the tops of the alkanethiolate chains, thus allowing direct imaging of the molecular lattices.[6,26,27] Under these conditions, the monolayers could be scanned repeatedly with no indications of destructive imaging.

2.3 Density Functional Theory Quantum Chemical Calculations. Density functional theory (DFT) calculations were performed to assist in the mode assignments and to define in detail the vibrational mode response of **2** when inserted into alkanethiolate monolayers of different lengths. To use computational resources efficiently for the latter task, nitrobenzene was used as a model molecule and the presence of the surrounding dielectric medium was represented using the Onsager dipole−sphere model.[28] Computations were carried out on a single node of an IBM SMP604e using the Gaussian-94 implementation of density functional theory.[29] The B3LYP functional, coupled with the 6-31G* basis set, was used since previous investigators have reported accurate vibrational mode calculations with this method.[30] Diffuse functions for nitrogen atoms were included for improved accuracy.[31] For the case of nitrobenzene modes, we find that the 6-31+G* basis set yields a root-mean-square deviation of 18.2 cm^{-1} from reported experimental values[32] when scaled by the recommended (see ref 30a) factor of 0.961. In general, the computations were carried out in the following steps: (1) optimization of a C_{2v} geometry starting from standard bond angles and lengths,[33] (2) electron density stability check, (3) frequency calculation and true geometric minimum check,[34] (4) calculation of the volume, (5) reoptimization of the geometry using the SCRF formalism with an appropriate dielectric constant, and (6) frequency calculation using the SCRF formalism with the appropriate dielectric constant. Since stable electron density distributions could not be obtained with the constraint of symmetric α- and β-spin electron densities, all calculations were performed without this constraint. The calculated frequencies then were assigned to specific modes in the Wilson−Varsanyi classification[35] via symmetry analyses and animation simulations using Hyperchem 5.0 software (Hypercube, Inc., Waterloo, Ontario, Canada).

3. Results and Discussion

3.1. Pure 2 Monolayers. *3.1.1 Ellipsometric Thicknesses: Difficulties in Obtaining Realistic Values for a Pure Monolayer Model.* Monolayers of **2** were assembled on Au/Cr/SiO$_2$/Si substrates by immersion in 0.03 mM solutions of **2b** in THF for 18 h with added base. Measurement of eight different samples gave average bare gold ellipsometry angles of $\Delta,\Psi =$ 109.75($\pm$0.08), 43.83($\pm$0.04)°, corresponding to a complex pseudo-dielectric constant of $-12.5274 + 1.1667i$. After self-assembly the average Δ,Ψ values were 107.52($\pm$0.08), 43.66-

Spectroscopic Characterization of Mixed Surface Assemblies

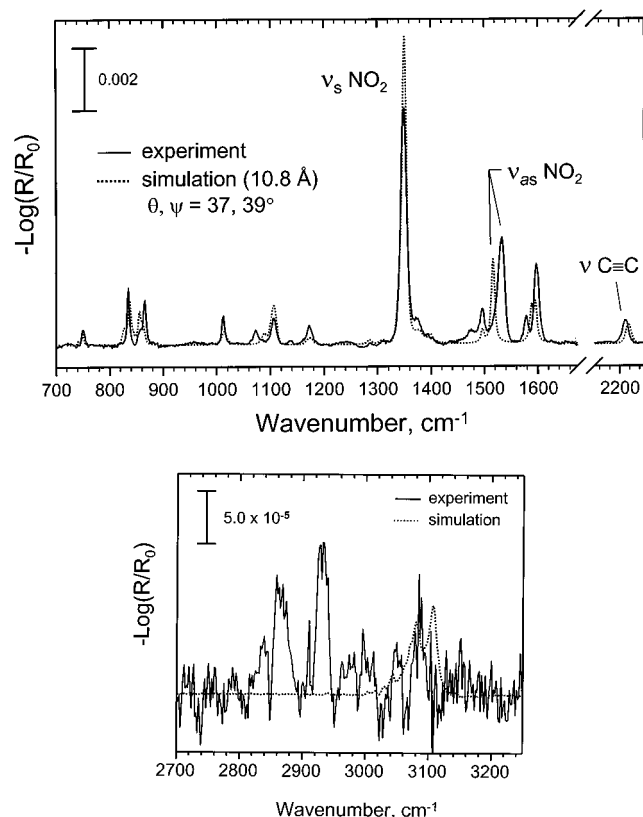*J. Phys. Chem. B, Vol. 104, No. 20, 2000* **4883**

Figure 2. (a) Low and (b) high frequency region infrared spectra of **2** self-assembled on gold: (—), experiment; (· ·) simulation using the anisotropic optical tensor derived from spectra of the bulk polycrystalline state of molecule **2b** with a model based on a 10.8 Å thick layer and an average molecular tilt and twist of 37 and 39° (θ, ψ, see Figure 1), respectively.

TABLE 2: Summary of the Peak Frequencies, Transition Dipole Moment Directions and Intensities of Selected Vibrational Modes of 2 in the Pure SAM Spectrum and in a Simulated SAM Spectrum Based on Optical Function Data Derived from the Bulk 2b Polycrystalline State

mode description[c]	peak frequency, cm^{-1} bulk	peak frequency, cm^{-1} SAM	transition dipole direction	I_{exp}[b]	I_{exp}/I_{iso}[b]
C≡C str	2218	2211	Z	0.76	2.25
C=C tang str (ν_{8b})	1594	1597	X	2.56	1.58
C=C tang str (ν_{8a})	1588	1579	Z	0.78	1.49
antisym NO$_2$ str (ν_a NO$_2$)	1519	1533	X	3.32	1.18
C=C str (ν_{19a})	1497	1496	Z	0.94	2.84
sym NO$_2$ str (ν_s NO$_2$)	1344	1349	Z	7.60	1.71
(ν_{9a})	1171	1172	Z	0.61	5.30
(ν_{13})	1106	1107	Z	0.85	1.56
(ν_{18b})	1089	1073	X	0.41	0.76
(ν_{18a})	1009	1012	Z	0.91	3.95
aryl C—H op r$_1$[d] (ν_{17b})	861	866	Y	1.50	1.31
NO$_2$ scissors (γ)	856, sh	857, sh	Z	0.38	sh only
∼ν_1 w/ −C≡C− str	837	834	Z	1.94	2.54
aryl C—H op r$_2$ (ν_{17b})	823		Y	0.05	0.06
NO$_2$ wag (β)	750	750	Y	0.49	0.42

[a] Assigned from the symmetry of the mode. The directions are shown in Figure 1, Z is parallel to the long molecular axis, X is perpendicular to Z and in the plane of the phenyl rings, and Y is perpendicular to the ring plane. [b]I_{iso} is the peak intensity [−log(R/R_o)] of the simulation for a 10.8 Å isotropic film. I_{exp} is the experimental intensity from the monolayer spectra. Intensities are scaled by 10^3. [c]Mode descriptions are in terms of Wilson's terminology for aromatic rings. Abbreviations: st = stretch, tang = tangential, sym = symmetric, asym = asymmetric, op = out of plane. [d]r$_1$ and r$_2$ represent the rings with the nitro and sulfur moieties, respectively. [e]No peak detected; the intensity is set to the noise level.

($\pm$0.04)°. Attempts to interpret these data in terms of isotropic, and even more rigorous anisotropic, models resulted in average thicknesses greater by as much as 20−30% (inherent experimental errors are $\pm$7−15%) than physically possible for the length of the molecule (see Table 1). Contributing factors to this discrepancy could include unexpectedly high packing densities, electronic perturbations of the Au−S interface caused by the electron withdrawing character of the NO$_2$ group,[36] as well as experimental difficulties in removing traces of hydrocarbon contamination in the monolayer (see below).

3.1.2. Infrared Spectra: The Presence of Contaminants and The Determination of Molecular Orientation. Figures 2a and b show the low- and high-frequency region IRS spectra, respectively. The aromatic ring C−H stretching mode intensities in the high-frequency region (>3000 cm^{-1}, Figure 2b) are too close to the intrinsic noise level to allow structural interpretations. Note also the presence of trace intensities of alkyl C−H stretching modes (2800−3000 cm^{-1}). Since **2** has no alkyl groups, the latter result shows the presence of submonolayer amounts of adsorbed hydrocarbon contaminants. From the optical functions of typical hydrocarbons we estimate that the band intensities are equivalent to those that would result from ∼2−3 Å of a disordered hydrocarbon-like contaminant. Extensive solvent washing of the samples never completely succeeded in removing these spectral features. Since the estimated amount of contamination closely matches the discrepancies in the ellipsometric thickness calculations, tenacious contaminants could be a significant contribution to the high SWE thickness values.

The low-frequency spectrum (Figure 2a) exhibits strong

features expected for **2**. The major peaks with their mode assignments and frequencies are summarized in Table 2 along with data taken from transmission spectra of dispersions of polycrystalline **2b** in KBr matrices. Typically we analyze these data to determine molecular orientation by (1) constructing anisotropic optical function tensors [$(\hat{n}_{ij}(\tilde{\nu}))$] from the isotropic KBr dispersion spectra and the transition dipole directions (Table 2),[22] (2) constructing different models with varied molecular orientations at the surface, in conjunction with independently measured film thicknesses, and (3) simulating spectra until a best-fit match with experiment is reached. In the present case, two factors necessitated a different approach. First, an accurate film thickness value was not available (from SWE, see above). Second, the observed frequency shifts between the SAM and the polycrystalline bulk for several important modes (e.g., NO$_2$ stretch; see data in Table 2) suggest that corresponding perturbations of the intrinsic intensities (oscillator strengths) could exist.[37]

The first problem of an inaccurate SAM thickness value is avoided by analyzing the peak intensity ratios for modes with different transition dipole directions within the experimental spectrum. These ratios are then compared to the corresponding ratios in a reference spectrum of an unoriented (isotropic) SAM. The reference spectrum is generated by a simulation based on a ∼1 nm (arbitrary) thick layer with an isotropic (scalar) optical function spectrum [$\hat{n}(\tilde{\nu})$] derived from the polycrystalline **2b** in KBr.[22] The second problem of errors in the intrinsic mode intensities was minimized by a global fitting procedure. This approach holds when the pattern of deviations of the polycrystalline state from the monolayer state is random so that the fluctuations in derived orientation angles from each mode around the correct ones approach complete cancelation in the limit of a large number of oscillators. Given the 15 normal modes distributed among the X, Y, Z molecular directions (Table 2), this condition is approximated.
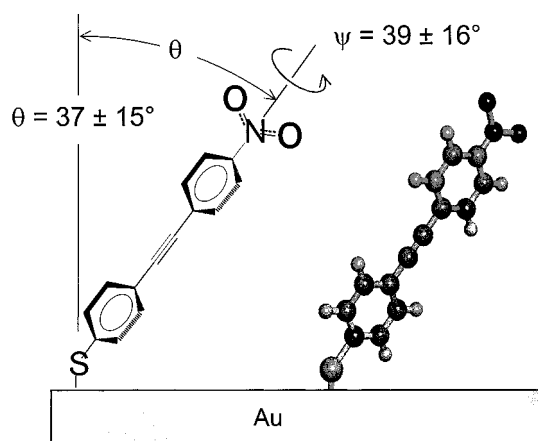
Figure 3. Cartoon showing the average orientation of a molecule of **2** in a pure SAM of **2**.

In the analysis, the intrinsic strength (transition dipole magnitude) of each mode was first factored out of the experimental peak intensities (I_{exp}) by normalizing to the simulated peak intensities of the isotropic (no net orientation; $\sim$10 Å film thickness) film (I_{iso}) to give $(I_{exp}/I_{iso})_j \equiv I^j_{\theta\psi}$ for the jth mode. The ratios are shown in Table 2. They were grouped into sets ($I^{jX}_{\theta\psi}$, $I^{jY}_{\theta\psi}$ and $I^{jZ}_{\theta\psi}$) according to the oscillator transition dipole directions (Table 2), and each of these sets then was averaged to give $\bar{I}^X_{\theta\psi}$, $\bar{I}^Y_{\theta\psi}$ and $\bar{I}^Z_{\theta\psi}$. For the fixed film thickness, these quantities are proportional to the square of the projections of the transition dipole moment components on the spectrally active laboratory Z_0 axis (Figure 1)[18,22] so $\bar{I}^X_{\theta\psi} \propto \sin^2(\bar{\theta})\cos^2(\bar{\psi})$, $\bar{I}^Y_{\theta\psi} \propto \sin^2(\bar{\theta})\sin^2(\bar{\psi})$ and $\bar{I}^Z_{\theta\psi} \propto \cos^2(\bar{\theta})$. Since the proportionality constants are all equal (the actual values scale with the simulated layer thickness), they can be factored out (thus also factoring out the simulated film thickness) and the remaining relationships yield $\bar{\theta},\bar{\psi} = 37(\pm15), 39(\pm16)°$. The errors were set by the standard deviations of the $\bar{I}^X_{\theta\psi}$, $\bar{I}^Y_{\theta\psi}$, and $\bar{I}^Z_{\theta\psi}$ values.

This analysis was checked by a simulation of an oriented SAM on the basis of a model with the above orientation angles and an optical response given by the anisotropic optical tensor $[(\hat{n}_{ij}(\tilde{\nu}))]$ (see above). The film thickness was set at 10.8 Å, as calculated from the molecular length of **2** (Table 2) and the tilt angle [13.5(cos 37°)]. The result is shown in Figure 2a, where frequency shifts and amplitude changes in the SAM spectrum (solid line), relative to the simulated spectrum based on the polycrystalline bulk state (dotted line), are observed. Note that the intensity mismatches are those associated with a global minimization of the variations in molecular orientation from mode to mode; the variations are both positive and negative. The issue of medium-induced vibrational mode perturbations will be treated in a quantitative way in the next section for the case of inserted **3** molecules in alkanethiolate SAMs.

An illustration of the corresponding structure of the pure **2** SAM is given in Figure 3. The tilt and twist values are within 10° of those reported for pure alkanethiolate SAMs with chains sufficiently long to show a high degree of conformational order.[15]

Despite repeated efforts, monolayers of pure **2** on Au/mica samples could not be imaged with molecular resolution. This result could indicate a lack of translational order. It is also consistent with the presence of adsorbed contaminants.

3.2. Alkanethiolate Monolayers with inserted 2. *3.2.1. Matrix Effects on Guest Molecule Orientation and Insertion Kinetics.* SAMs of the pure alkanethiolates were immersed into
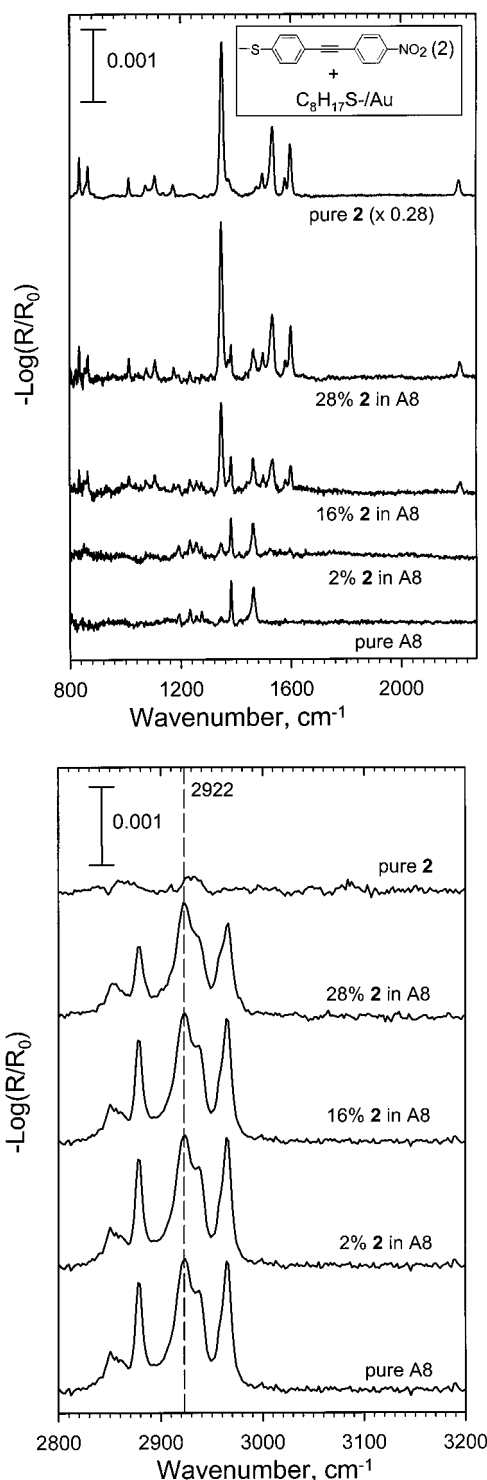

Figure 4. (a) Low- and (b) high-frequency region IRS spectra of host **A8** SAMs containing different amounts of inserted **2** molecules. For reference, spectra of a pure **2** SAM and an **A8** SAM are also shown. (a) In the low-frequency spectra, the near invariance of the relative mode intensities of **2** with film composition indicates that the orientation of **2** is constant in all films. The high-frequency spectra in b show that the insertion of **2** has only a small effect on the C−H stretching signature of the **A8** matrix SAM. The dashed line shows that the d⁻ mode position remains constant despite the amount of **2** inserted.

0.03 mM, basic THF solutions of **2b** for selected amounts of time and rinsed according to the standard procedures. Typical IRS spectra for **2** inserted into an **A8** SAM are summarized in Figure 4. Similar data were obtained for **2** inserted into **A10**, **A12**, and **A14** SAMs.
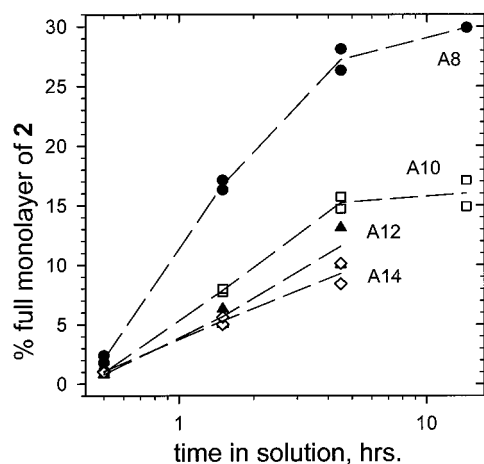
Spectroscopic Characterization of Mixed Surface Assemblies

J. Phys. Chem. B, Vol. 104, No. 20, 2000 **4885**

Figure 5. The degree of insertion of **2** molecules into alkanethiolate SAMs of differing thickness as a function of immersion time. The percentage was determined by scaling the intensity envelope of the pure **2** SAM spectrum until it matched the intensity envelope of the spectrum of the **A8** SAM with inserted **2**; the scaling factor is defined as the fraction inserted. The mode intensities of the $-NO_2$ ν_s, the $-NO_2$ ν_{as}, the out-of-plane ν_{17b} at 866 cm^{-1}, and the ethynylene stretch at 2212 cm^{-1} modes were used primarily in the comparison.

The fractions of inserted **2** were deduced from the low-frequency diagnostic modes (Figure 4a). The observation of a constant set of peak intensity ratios in a given spectrum for all dilutions of **2** in the **A8** SAM matrix and for the pure **2** SAM shows that the inserted molecule geometry does not change with composition. Thus, the amount of inserted **2** can be calculated as a simple ratio of the envelope of these intensities in the inserted **2** and pure **2** SAM spectra. For the shortest insertion time (0.5 h), only the 1350 and 1530 cm^{-1} modes were distinguishable from the noise. On the basis of these modes, the detection limit of inserted **2** is estimated as ~0.5%. In general, there is very little perturbation of the line shapes and positions of the alkyl C–H stretching region upon insertion of **2** (Figure 4b). This result is consistent with overall retention of order in the host SAM matrix upon insertion of **2**.[5]

The percentage of inserted **2** vs time is plotted in Figure 5. These data show an inverse dependence of insertion rate on the alkanethiolate chain length, with the sharpest change between **A8** and **A10** SAMs. Using this dependence allows accurate control of the inserted fraction of guest molecules. On the basis of previous studies,[38] the rate-determining step for exchange should involve displacement of the chemisorbed alkanethiolate by **2a** (thiol) with release of an alkanethiol molecule. Our STM results, both the present (see below) and previously reported[5,6] ones, confirm that the exchange preferentially occurs in defect regions. The observed decrease in rates with increasing chain length suggests a corresponding decrease in the monolayer defect content and/or an increase in chain packing in the defect regions between **A8** and **A14** SAMs. The enhanced drop in insertion rates between **A8** and **A10** is consistent with previous IRS and electrochemistry observations of enhanced increases in packing and electrochemical blocking in progressing through this chain length region.[39] These effects must be subtle, however, since inspection of our STM data of the pure alkanethiolate SAMs show no obvious trends in the defect counts or types within the errors of the image resolutions (see below).

3.2.2 Molecular Resolution Topographies by Scanning Tunneling Microscopy. STM images were taken before and after the immersion of the alkanethiolate SAMs in the solutions of **2b**. In all cases, the initial SAMs provided the expected molecular resolution images of the alkanethiolate molecules.[40,41]

Images of alkanethiolates of different lengths containing inserted **2** are shown in Figure 6 and are typical of hundreds of ones recorded. Note the crystalline order of the *n*-alkanethiolate monolayers (e.g., in Figure 6c) as well as the typical deposition-induced Au substrate vacancy ("pit") defects (dark areas). Figure 6a also shows a SAM terrace domain boundary (upper left). Protruding from the film are features (bright spots) that we assign to **2**. As expected from our previous results with molecule **1**,[6] the inserted **2** molecules are inserted both individually and in clusters at step edges and terrace domain boundaries, sites where the film density is decreased. We find this pattern of insertion to be generally independent of the host SAM thickness, as illustrated by comparisons between Figures 6a–d. The decreased quality of molecular resolution in the image for the **A14** host matrix (Figure 6d, shown at greater magnification to reveal the individual molecules), relative to the shorter alkanethiolate SAMs, arises from approaching the limit of detectable tunneling current for this thickest SAM.[9] Immersion of the alkanethiolate SAMs in the basic solutions of **2b** for extended periods results in occasional insertion into the interiors of the ordered alkanethiolate domains on {111} terraces, as shown for an **A12** SAM in Figure 6c. From analysis of many images, we estimate that <1% of the insertion events occur in these regions. The exact mechanism of the exchange remains uncertain and requires further study to be defined.[42]

3.2.3. Chemical environment of the terminal $-NO_2$ group of inserted 2. On the basis of the similar tilt angles for inserted **2** molecules (~40°) and the alkanethiolate chains (~30°) and the relative molecular lengths, the local environment of an inserted **2** molecule should range between partial protrusion above and complete immersion in the host SAM matrices. Cartoon structures of the two limiting cases of the **A8** and **A14** SAMs are shown in Figure 7. In the lower part of the figure, structures **A** and **B** associated with the **A14** SAM case represent possible types of limiting variations in local environments. Also shown are cartoon representations of the STM line–scan trajectories. While the pictures in Figure 7 are not accurate overall, they are roughly to scale in the vertical direction with regard to the film–molecule structures and the peak heights of the STM line scans, Δh_{STM}. Plots of the measured Δh_{STM} values are shown in Figure 8 as a function of the alkanethiolate chain length. For comparison, the heights of the top of the NO_2 group above the host SAMs were determined from molecular models for an ideal structure of **2** incorporated in a uniformly tilted domain on a {111} terrace region.[43] These model structures for the **A8** and **A14** SAMs are shown at the bottom of the figure and the Δh_{model} values for all the SAMs are given in the plot. The significant difference between Δh_{STM} and Δh_{model} underscores the fact that STM data are a convolution of electronic and steric effects and cannot be used directly to characterize molecular topographies.[7a,9]

It is of fundamental importance for understanding the intrinsic conductance properties of EAMs to unravel these types of tunneling–structure correlations. To do this it first is necessary to characterize the actual local electronic environment(s) of the inserted molecules since these environments could influence the electron tunneling probabilities in the region of the molecules.[9] As suggested by structures **A** and **B** in Figure 8, there can be significant variations in the density, and thus electrical properties, of the local medium surrounding an inserted molecule. Molecular vibration frequencies are well-known to be sensitive to variations in the medium.[44] Accordingly, note the smooth, monotonic decrease of the $\nu_s(NO_2)$, $\nu_a(NO_2)$, ν C≡C, ν_{8b}, ν_{8a}, and ν_{19a} peak frequencies with increasing alkyl chain length shown in the plots in Figure 9 (original spectra not shown except
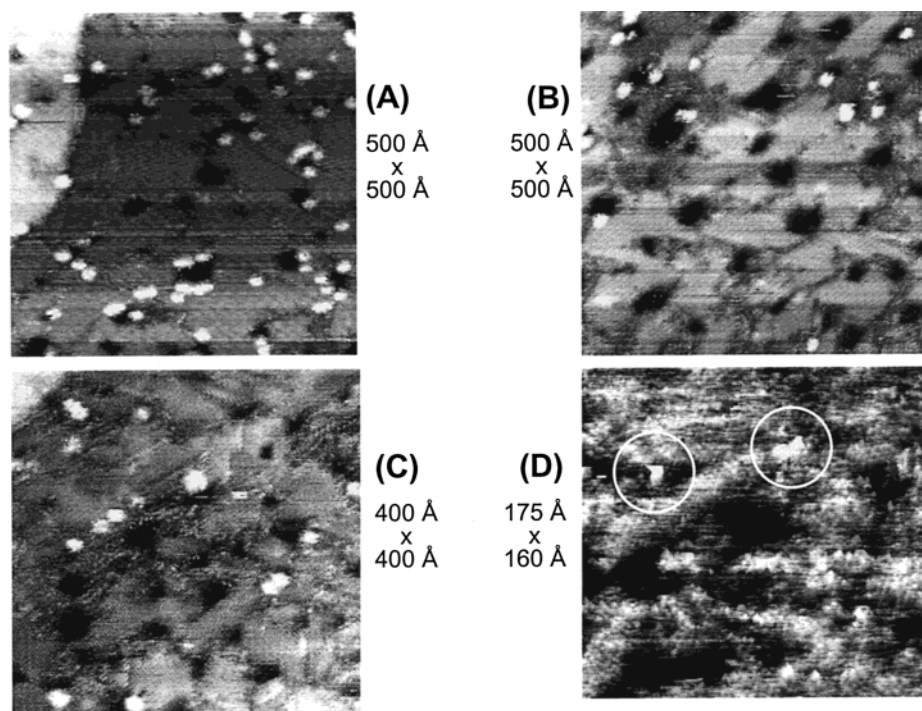
Figure 6. STM images of **2** inserted into (a) **A8**, (b) **A10**, (c) **A12,** and (d) **A14** SAMs. Substrate vacancy defects, terrace boundaries, and alkanethiolate lattices are visible. The **2** molecules appear at domain boundaries on the terraces. The tunneling conditions were tip bias +1.0 V and between 2 and 5 pA tunneling current. Since the tunneling currents for the **A14** SAMs are near the limit of the signal-to-noise of the current measurement, image **6d** is shown at higher magnification in order to better reveal the individual molecules (see text).
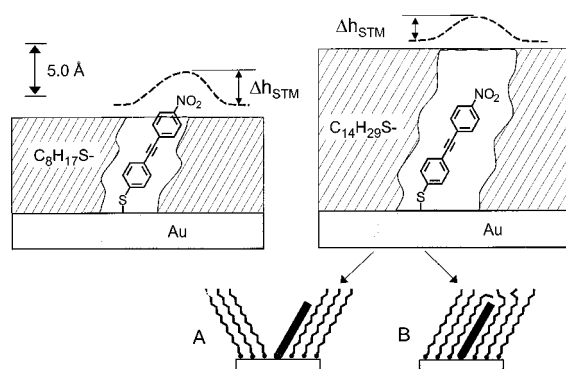

Figure 7. Schematic structures of the two limiting cases for insertion of **2** into **A8** and **A14** SAMs. Also shown are cartoon representations of the STM line-scan trajectories (dashed lines). Structures **A** and **B** associated with the **A14** SAM case represent possible types of limiting variations in local environments.

for the **A8** SAM in Figure 4a). These data qualitatively parallel the observed frequency changes in going from a gas to a condensed phase for nitrobenzene, e.g., 1355−1347 cm^{-1} for $\nu_s(NO_2)$.[45] The $\nu_s(NO_2)$ and $\nu_a(NO_2)$, modes of **2**, were sufficiently strong to be visible in all of the compositions examined. For these modes, the peak frequencies were observed to be independent of the insertion fraction for each of the different alkanethiolate chain length SAMs. Thus, the shifts with matrix chain lengths (Figure 9) indicate that the local environments of the NO_2 groups are a function of only the matrix SAM thicknesses.

To understand more quantitatively the connection between these spectral changes and changes in molecular environment, DFT quantum chemical calculations were performed to generate theoretical values of the $-NO_2$ vibrational frequencies for immersion in two uniform media with different dielectric constants ϵ. For computational efficiency, nitrobenzene was chosen as the probe molecule and the oscillator-medium
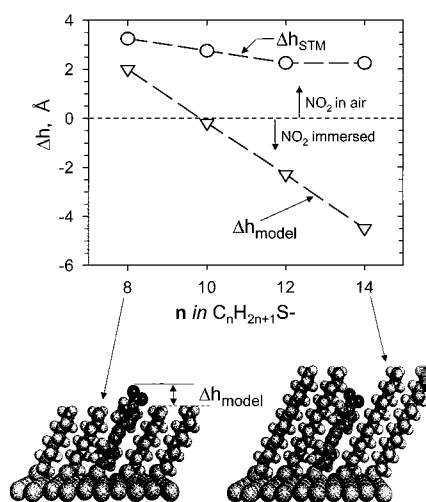

Figure 8. The graph illustrates the contrast between the measured constant-current height of the **2** features above the alkanethiolate matrix (Δh_{STM}, ○) with the geometric height difference expected from a simple hard-sphere model (Δh_{model}, △). Also shown below are projections of space-filling models of **2** in **A8** (left) and **2** in **A14**.

interaction was treated using the Onsager dipole−sphere model.[28] Calculations were done with two limiting media: air ($\epsilon = 1.0$), representing the **A8** SAM case, and a condensed hydrocarbon phase ($\epsilon = 2.02$), representing the buried case of the **A14** SAM.

The calculation results are represented in Figure 9 by arrows where the length shows the magnitude of the shift and the direction shows a change from the gas-phase to the condensed hydrocarbon media. The calculated shift directions all match those of the same modes of inserted **2** while the calculated magnitudes match well for all but the ν_{19a} ring mode. Considering just the NO_2 mode shifts, the good fit of theory combined with the smooth dependence of frequency on alkanethiolate length, strongly suggest that, on average, the alkanethiolate
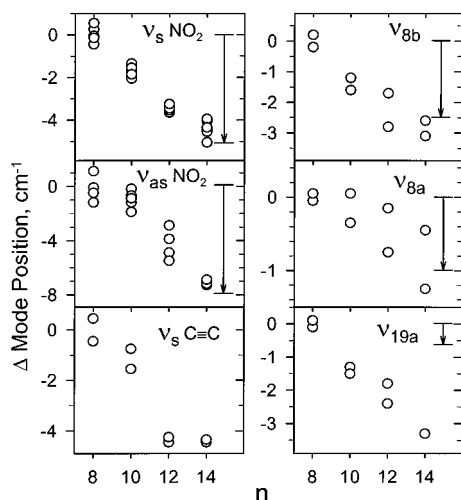
Spectroscopic Characterization of Mixed Surface Assemblies

J. Phys. Chem. B, Vol. 104, No. 20, 2000 **4887**

Figure 9. Plots of vibrational mode frequencies of inserted **2** as a function of the total number of carbons in the alkyl chain of the host SAM matrix. Six easily observed modes are shown. For each mode, with the exception of the $-C\equiv C-$ stretch, a theoretical calculation of the relative peak shift of the corresponding mode in nitrobenzene was performed. The B3LYP functional was used with the 6-31+G* basis set and Onsager's SCRF dipole–sphere formalism was used to simulate air and hydrocarbon dielectric environments ($\epsilon = 1$ and 2.02, respectively). The arrow direction indicates the frequency shift direction for $\epsilon = 1 \rightarrow 2.02$, while the magnitude indicates the size of the shift. See text for details.

chains remain uniformly collapsed around the NO_2 group as its extent of immersion increases with increasing alkanethiolate length. This picture fits with a structure such as **B** in Figure 7. Keeping in mind that the STM data show that insertion occurs predominantly at film defects (see above), it is important to note that the IRS data show that the host matrix around these defect sites must be sufficiently dense, on average, to collapse significantly around the inserted molecules.

Inspection of the ideal model structures in Figure 8 shows that while the NO_2 group of **2** is clearly moved from a gas-phase to an immersed environment between the **A8** and **A14** SAMs, the aromatic portion retains a primarily hydrocarbon-like environment. In apparent contrast, the plots in Figure 9 show ring mode (ν_{8a}, ν_{8b}, and ν_{19a}) shifts with changes in the SAM matrix. This effect can be understood on the basis of a strong coupling between the rings and the NO_2 group, as indicated by our analysis of the DFT calculations for nitrobenzene. This result shows an interesting effect in which vibrational modes of immersed molecular units can be sensitive to changes in the adjacent medium as relayed by as a coupled terminal group, especially a highly polar group such as NO_2. The discrepancy between the calculated and observed shifts for mode ν_{19a} is likely due to the limitations of nitrobenzene (one ring) as a model for **2** (two rings).

In all scans, the STM tip remains continually outside the alkanethiolate film as it moves across the surface. Therefore, given the above conclusion that the hydrocarbon chains of **A10** and higher SAMs collapse around the inserted **2** molecules, it is clear that the vertical tip to ground tunneling path must switch from tip/vacuum/**2**/Au to tip/vacuum/hydrocarbon/**2**/Au in going from **A10** to **A12** and higher SAMs. This helps to understand the slow falloff in Δh_{STM} in Figure 8. The tunneling current falloff with tip–substrate separation is faster for tunneling through vacuum than an alkanethiolate chain.[9,46] Thus, the appearance of an intermediate hydrocarbon medium in the longer SAMs will cause the tip to move further from the substrate than if no molecules were present beyond **2**. This
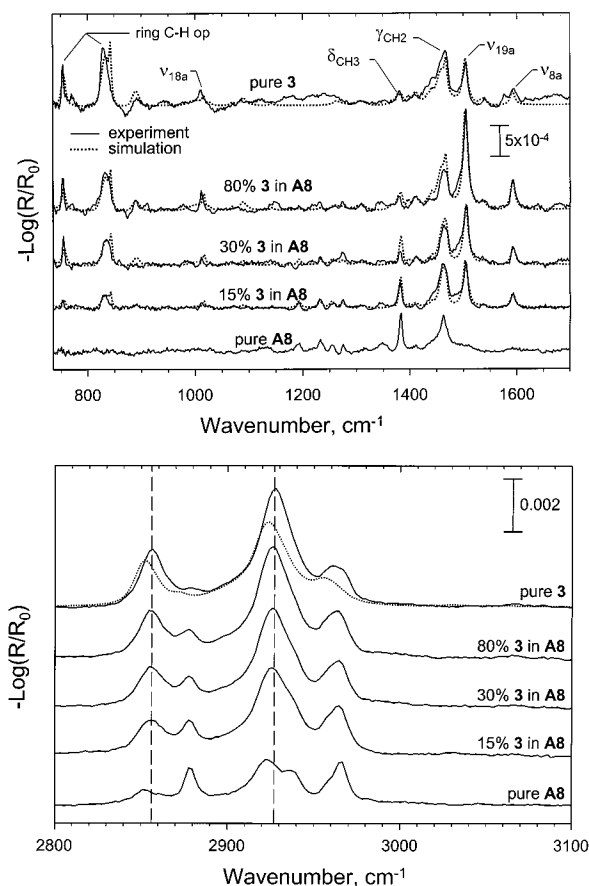

Figure 10. (a) Low- and (b) high-frequency region IRS spectra of **A8** SAMs with inserted **3** molecules and pure **3** and pure **A8** SAMs. The mixed SAMs are labeled according to the percentage insertion of **3** molecules as determined from analysis of the SWE and IRS data (see text). Simulated spectra (· ·) are included. The simulations were based on anisotropic models of domains of oriented molecules and the heterogeneity of the films was treated using the Maxwell–Garnett effective medium approximation. The molecular orientation angles are the best-fit values taken from a combined analysis of the SWE and the IRS data (summarized in Table 4). The simulations for the mixed and the pure **3** SAM are shown in the (a) low-frequency region; (b) only the pure **3** SAM simulation is shown in the high-frequency region. The d^+ and d^- mode experimental peaks in **b** are marked by the dashed lines at 2856 and 2927 cm^{-1}, respectively.

compensating effect leads to a flattening of the Δh_{STM} vs chain length curve, as observed.

3.3. Pure 3 Films. Monolayers of **3** were created by immersion of clean gold surfaces into basic solutions of 0.017 mM **3b** in THF for 18 h. Longer deposition times resulted in no further changes in the film characteristics determined from IRS and SWE measurements. Further, STM imaging showed no evidence of ordering, as observed for the pure **2** SAM. Assuming that no contaminants are present and using an average (isotropic) refractive index, the SWE data yield an average (four samples) film thickness of 23($\pm$2) Å. Given the total molecular length of ~40 Å (Table 1), the data indicate a substantial tilt of the long molecular axis [$\theta = \cos^{-1}(23/40.2) \sim 55°$].

The low-frequency IRS spectrum in Figure 10a (top) shows prominent features (refer to Table 3) at 1504 [ν_{19a}], 1467 [γ (CH$_2$); C$_{12}$H$_{25}-$ side chains] and 834 and 754 cm^{-1} [ring C$-$H out-of plane]. Because of the presence of the strong C$-$H modes from the alkyl side chain in the molecule, it was not possible to conclude whether trace hydrocarbon contaminants were present in the SAM (see above discussion for the pure **2** SAM). Spectral simulations were made using optical tensor spectra

TABLE 3: Summary of the Peak Frequencies and Transition Dipole Moment Directions of Selected Vibrational Modes of 3b in the Bulk Polycrystalline State and 3 in the Pure SAM

	peak frequency, cm^{-1}		transition dipole direction[a]
mode description[b]	bulk	SAM	
asy CH$_3$ str (r$_a$-)	sh	2961	c
asym CH$_3$ str (r$_b$-)	2955, w	sh?	c
antisym CH$_2$ str (d$^-$)	2922, vs	2927	c
sym CH$_3$ str (r$^+$)	2871, w	2880	c
sym CH$_2$ str (d$^+$)	2852, vs	2856	c
C≡C str ($v_{C≡C}$)	2207, w	not obs	Z
C≡C tang str (v_{8a})	1592, m	1595	Z
C≡C str (v_{19a})	1504, vs	1504	Z
CH$_2$ bend (γ CH$_2$) of C$_{12}$H$_{25}$− side chains	1467, s	1466	c
C≡C str (v_{19b})	1411, w	not obs	X
δ_s −CH$_3$ of C$_{12}$H$_{25}$− side chains	1384, w	1381	c
C≡C str (v_{18a})	1016, w	1011	Z
C−H op	842, s	sh	Y
C−H op	834, vs	829 + sh	Y
C−H op	755, s	754	Y

[a] Assigned from the symmetry of the mode. The directions are shown in Figure 1, Z is parallel to the long molecular axis, X is perpendicular to Z and in the plane of the phenyl rings, and Y is perpendicular to the ring plane. [b] Mode descriptions are in terms of Wilson's terminology for aromatic rings. Abbreviations: st = stretch, tang = tangential, sym = symmetric, asym = asymmetric, op = out of plane. [c] The alkyl mode directions are not defined because of the possible conformational variations of the chain units.

derived from KBr dispersions of pure **3b** with the film thickness approximated by the above ellipsometric value. Using the 1595, 1504, 834, and 754 cm^{-1} modes as a primary diagnostic, the best-fit simulation, shown in Figure 10a, was obtained with θ, ψ = 62($\pm$3), 44($\pm$7)°.[47] The fit of the out-of-plane modes is not as good as the fit of the long axis (Z) ones, largely as a result of a peak width change between the isotropic reference (~8 cm^{-1} fwhm) and monolayer (~4 cm^{-1} fwhm) states for the 754 cm^{-1} mode. The approximate fit of the CH$_2$ scissors mode peak of the C$_{12}$H$_{25}$− side chain should be viewed as a coincidence since the polycrystalline reference state does not accurately model the average conformational state of the alkyl chains. This can be seen in Figure 10b (top) by comparing the simulated spectrum, based on a model of a 23 Å thick isotropic film of pure polycrystalline **3b**, with the experimental monolayer spectrum. The frequencies of the d$^-$ and d$^+$ modes (2923 and 2852 cm^{-1}) in the isotropic reference spectrum are between those expected for a solid (crystalline, all trans) and liquid (disordered) alkane,[48] indicating that the side chains are disordered in the pure compound (also see Table 3). In contrast, the SAM d$^-$ and d$^+$ peaks are 4 and 3 cm^{-1} higher, respectively, than the isotropic spectrum values. This shift indicates that the chains in the experimental monolayer are approaching conformations characteristic of a liquid alkane. Since the intrinsic oscillator strengths of the C−H stretching modes will vary with the degree of conformational order,[49] the polycrystalline state is thus not an accurate reference for the side chains in the SAM. The lower intensity of the simulated spectrum relative to that of the pure SAM (Figure 10b) is consistent with this conclusion.

3.4. Alkanethiolate Monolayers with Inserted 3. *3.4.1. Matrix Effects on Guest Molecule Orientation.* The insertions were carried out by immersion of the **A8** SAMs into 0.017 or 0.17 mM THF solutions of **3b** with added base four times ranging from 0.5 h to several days.

3.4.4.1. Ellipsometry Data and Low-Frequency Infrared Spectra: Analysis of Film Composition and Molecular Orienta-

tion of Inserted 3. The low-frequency spectra in Figure 10a reveal that the ratios of the peak intensities of the aromatic ring C−H out of plane modes (Y mode, Table 3) to the ring stretching modes (1500−1600 cm^{-1}, Z mode) differ considerably between the pure **3** SAM and the mixed SAMs. Qualitatively, this suggests that the molecular orientation of **3** is different in mixed monolayers as compared to the pure monolayer environment. Quantitatively, this means that the intensity envelope of the spectral modes of **3** cannot be scaled directly to determine the extent of insertion, in contrast to the cases of the inserted **2** SAMs. For this reason, determination of film composition and molecular orientations was accomplished by a concerted analysis of the IRS and SWE data. The latter proved to be useful since substantial changes in the measurements occur for even small inserted fractions of the large **3b** molecule in the matrix of the relatively small alkanethiolate molecules. The SWE Δ, Ψ values for the three films before and after insertion are summarized in Table 4. The samples are labeled according to the values of the final best-fit composition (see below). Note that since Ψ is experimentally nearly invariant with the extent of insertion, for each SWE measurement Δ effectively is the only experimentally measured quantity useful for analysis. Thus, in a given SWE analysis all parameters associated with each model must be independently known except the one to be determined.

The three general levels of models considered are summarized in Figure 11. Since the IRS data indicate that the **3** molecules are oriented while the STM data (see below) show that some fraction of these must exist as single, isolated molecules, the most accurate model would be based on some combination of the two heterogeneous film models, **II** and **III**. Because of the number of undefined parameters associated with this approach,[50] we chose to utilize model **II** and the simplified version, model **I**, in which the optical functions of the domains of oriented **A8** and **3** molecules were assumed to be optically isotropic (viz., $\hat{n}_{xx} = \hat{n}_{yy} = \hat{n}_{zz}$). For both models the spatially heterogeneous character of the film was treated explicitly using the Maxwell−Garnett effective medium approximation (EMA).[21] The overall approach to determining the film composition and molecular orientation of inserted **3** involved: (1) generating a starting guess of the film composition by qualitative examination of either the SWE or IRS data, (2) using Model **I** with polycrystalline **3b** and **A8** isotropic optical functions to simulate IRS spectra which yield first values of the molecular orientation (θ, ψ) of inserted **3** by the spectral intensity ratio method (see section 3.2.1), (3) using ($d_1 + d_2$) calculated from cosè with the SWE data (Δ) in Model **I** to generate an improved film composition, (4) using the film composition and ($d_1 + d_2$) with the IRS data to generate a new best-fit θ, ψ set, and (5) returning to step 3 and reiterating until a stable set of film thickness, composition and orientation angles is obtained. The final set of parameters, summarized in Table 4, was checked by comparison of experiment and an IRS simulation using model **II**. Important aspects of the procedures are discussed below.

In the model **I** SWE analysis (step 3), both components were assigned the same scalar refractive index of $n = 1.50$[51] and $d_1 = d_{pureA8}$, where the latter was determined from the SWE data of the preinsertion **A8** SAM. Since $n_3 = n_{A8}$, an EMA was unnecessary for layer 2. The film composition is expressed conveniently as the fractional areal coverage $\sigma_3/(\sigma_3 + \sigma_{A8})$, where σ = the partial area occupied by a component in a saturation coverage film. The volume fractions of **3** and void in layer 1 are related, respectively, by: $f_3 = \sigma_3/(\sigma_3 + \sigma_{A8})$ and $f_{void} = (1 - f_3)$. Setting f_3 or $d_{film}/(d_1 + d_2)$ allows calculation of d_{film} or f_3, respectively, from a measured Δ value.[52]

Spectroscopic Characterization of Mixed Surface Assemblies

J. Phys. Chem. B, Vol. 104, No. 20, 2000 **4889**

TABLE 4: Summary of the Best-fit Molecular Orientation and Composition Results from Combined Analysis of the SWE and IRS Data for Films of 3 Inserted into A8 SAMs

sample[a]	ellipsometric parameters, Δ, Ψ, deg (bareAu, A8/Au, (3 in A8)/Au)	model I SWE analysis			model II IRS analysis[b]	
		$d_2 = d_{pureA8}$, Å	film thickness, $d_{film} = (d_1 + d_2)$, Å	fractional content of 3, f_3[c]	$\theta \psi$; deg[c]	film thickness, $d_{film} = 40.2\cos\theta$, Å
80%	109.63, 43.88 108.53, 43.68 106.96, 43.72	10.0	26.8	0.80(±0.13)	48(±3), 40(±10)	27.9
30%	109.24, 43.84 108.08, 43.68 107.35, 43.64	10.6	28.5	0.30(±0.07)	45(±3), 55(±9)	28.4
15%	109.87, 43.84 108.74, 43.68 108.33, 43.62	10.2	31.6	0.15(±0.03)	38(±4), 57(±11)	31.7

[a] Designation based on the f_3 values from the model II SWE analysis. [b] On the basis of the f_3 values from the model II SWE analysis and the spectra in Figure 10a. [c] Errors are based on the SWE measurement errors.

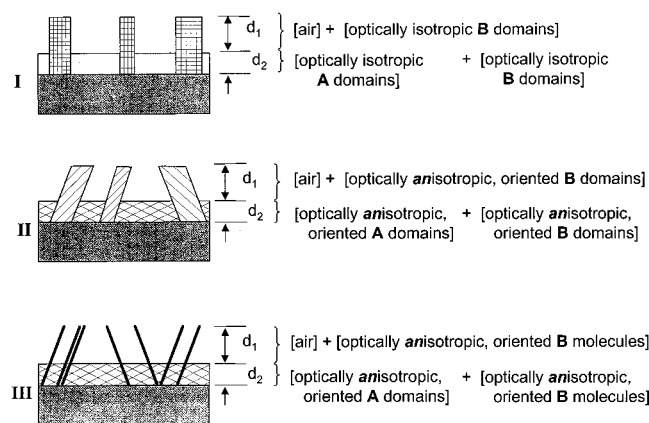**Figure 11.** Schematic representations of three different models considered for analysis of the SWE and IRS data of films formed from insertion of **3** in **A8** host SAMs. The pictures are intended to be aids in discussing the simulations and not to accurately represent the actual physical characteristics of the films.

Figure 12. The dependence of the average tilt angle (θ) of inserted **3** molecules in an **A8** host SAM on the percent insertion.

In the IRS simulations only the low-frequency region was considered. The EMA was applied to both layer 1 and layer 2 to determine the composite optical function spectra. In the step **2** simulation, the composite optical function of layer 1 was set up from the isotropic optical function spectrum of **3** molecules [$\hat{n}^3_{iso}(\tilde{v})$], determined from the bulk polycrystalline state, and an isotropic pseudo function of **A8** molecules [$\hat{n}^{A8}_{SAM}(\tilde{v})$] as they exist in the pure **A8** SAM.[53] Layer 2 was described by $\hat{n}^3_{iso}(\tilde{v})$ and n_{air} = 1.0. The resultant spectra represent a hypothetical film with unoriented **3** molecules in an oriented **A8** matrix. Analysis of the diagnostic bands of **3** in the experimental spectrum via the spectral intensity ratio method (see section 3.2.1), using the simulated spectrum as a reference, allowed determination of θ, ψ values. The final IRS simulation with model **II** used $\hat{n}^{A8}_{SAM}(\tilde{v})$; the anisotropic optical function tensor spectrum of **3** molecules [$\hat{n}^3_{ij}(\tilde{v})$], with the elements calculated using the final θ, ψ values; and the film thickness set as the final ($d_1 + d_2$) value. In all cases, the agreement obtained between the Model **II** IRS simulation and experiment checked the validity of the final parameters. Examples of fits are shown in Figure 10a for the cases of 15, 30, and 80% insertion. The poor fits of the alkyl-chain modes (CH₂ and CH₃ bending) are expected since the conformational states of the side chains vary with the surrounding environment and do not reflect the aromatic orientation in a smooth way. The self-consistency of the data can be seen in Table 4 by the nearly
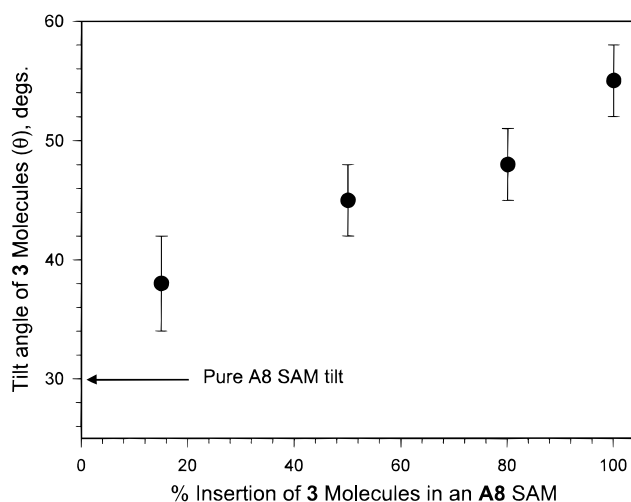
equal values of the film thicknesses determined from the SWE analysis and calculated from the tilt angles from the IRS analysis.

The above analysis shows that the average tilt angle of inserted **3** molecules decreases with decreasing extent of insertion in the **A8** host SAM (Table 4). This trend is shown in Figure 12. Note that as the molecules approach infinite dilution the tilt angles approach those of the chains in well-ordered *n*-alkanethiolate/Au{111} SAMs.[15] This suggests that the individual molecules observed in the STM measurements exhibit an average tilt close to that of the host SAM. The higher tilt angles in the pure **3** SAM may result from a strong tendency for the large, polarizble (extended π-system) molecules to adsorb in a flat configuration on the Au surface.[54] At low coverages alkanethiols adsorb to form flat (striped) phases while at higher coverages the tilted phase forms.[55] The self-assembly of pure **3** likely departs from this behavior in that once a molecule of **3** is initially adsorbed in a flat configuration, its strong surface interaction may not allow reconfiguration to a tilted structure as coverage increases. Thus, some initial fraction of molecules would remain in an irreversible flat configuration while subsequent molecules insert with tilted configurations in open surface regions to give a mixture of configurations exhibiting a higher average tilt than that of an ideal tilted phase.

3.4.4.2. High-Frequency Infrared Spectra: Analysis of Alkyl Side chain Structure on Inserted 3. The composite **3** and **A8** C−H stretching mode spectra of the mixed films are shown in Figure 10b. There is a slight trend toward higher frequencies in d⁻ mode peak position values as one increases in **3** insertion
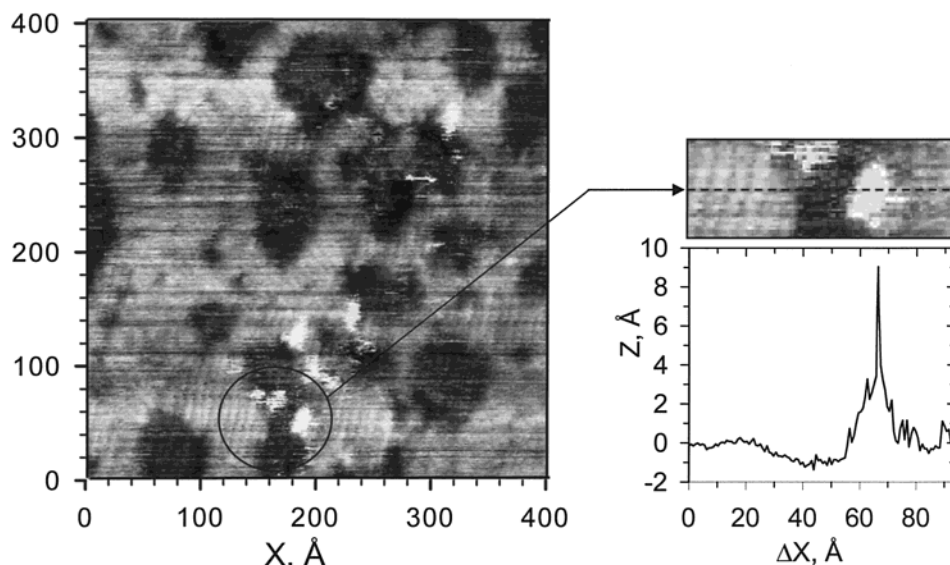
Figure 13. A representative STM image of a 400 Å × 400 Å area of an **A8** host SAM containing inserted **3** molecules. Also included is a line scan through one of the observed peaks. Current spikes with topographic heights ranging from 20 to 40 Å are observed as the probe tip passes the general features representing molecules of **3**. The tunneling conditions were +1 V bias and 3 pA tunneling current.

amount (from 2925 to 2926 cm^{-1} across the range of 15−80% inserted **3**). If one subtracts the residual **A8** from the mixed spectra then one obtains a d$^-$ mode peak position of 2926.5- (±0.3) cm^{-1}. This corresponds to an upward shift of ∼3 cm^{-1} of the residual **3** in **A8** d$^-$ mode peak relative to that of the bulk polycrystalline state. This residual **A8** subtraction method is somewhat crude, as there may be orientation changes to the **A8** as more **3** is inserted, especially at high insertion fractions. The magnitude of this shift suggests that the alkyl side chains of inserted **3** are more conformationally disordered, and thus less well packed, than in the pure polycrystalline reference state. The nearly identical shift observed for the pure **3** monolayer (top plot) suggests that the dominant state of inserted **3** is in the form of domains, as opposed to single, isolated molecules. In the latter case, the lack of neighbors for protruding chains would be expected to lead to significant differences in the chain packing. Consistent with this picture is the ability of the domain model (model **II** above) to provide reasonable fits to the IRS and SWE data. Thus, we conclude that single isolated molecules comprise only a small fraction of the inserted **3** molecules on polycrystalline Au substrates.

3.4.2. Molecular Resolution Topography by Scanning Tunneling Microscopy. Samples for STM analysis were created by dipping **A8** SAMs into solutions of 0.017 mM **3b** in THF with base for 5 min. The conditions were chosen to yield low insertion fractions so that a significant fraction of inserted molecules would be isolated. Companion samples did not show any insertion of **3** by SWE within experimental error (∼±1−2 Å), but the IRS spectrum showed the appearance of a weak peak at 1504 cm^{-1} and C−H stretching features in the C−H stretching region, thus confirming the insertion of **3**.

The STM images of these films consistently show elevated features among the typical substrate defects and terrace domain boundaries, as seen in Figure 13. Although the alkanethiolate lattice has not been fully resolved, rows representing the orientational domains of **A8** chains are visible. We assign the elevated features to inserted **3** molecules. Repeated scans show variations of the image shapes of the **3** molecules from spot to spot. As described earlier,[5,6] long protruding molecules have the effect of imaging the STM tip. Given the 40 Å molecular length of **3** together with a long axis tilt (refer to Figure 3) of $\theta \sim 35°$ (from extrapolation of the plot in Figure 12 to zero

insertion), the top of **3** protrudes ∼20 Å outside the **A8** SAM, akin to fence posts surrounded by grass. Line scans through these elevated features typically show ∼9 Å peaks (Δh_{STM}) sitting on a broad base with spikes emanating, typified by the scan of the selected feature in Figure 13. Occasionally the side spikes reach heights of as much as ∼40 Å above the baseline.[5] These spikes are never observed over regions of pure alkanethiolates. We ascribe the spikes to the STM feedback loop trying to respond as contact occurs with the complex-shaped conjugated molecule during the lateral scan.[5] For example, during the scan through the local vicinity, the STM tip may transiently distort the molecular configuration of the long oligomer by perturbing the molecular tilt and/or the alkyl side chain conformation with resulting jumps in the tip−sample distance. A schematic helpful for visualizing the latter possibility is shown in Figure 14. The mechanism for molecule contact should be very path dependent as the tip approaches the molecule and thus can be expected to produce variations in the spike pattern from scan to scan, as is observed. We note also that the oligomer features do not disappear or migrate across the film in these images. Thus, the oligomers are firmly bound to the substrate and are *not displaced* on the Au substrate surface by the tip.

We consistently observe that fully conjugated thiolate molecules tend to insert in defects of the host SAM matrix. We note that our SWE and IRS analyses (previous section) suggest that for polycrystalline gold **A8** SAMs the dominant mode of insertion of **3** molecules is in the form of bundles or domains. Given that the STM shows the presence of what appears to be individual **3** molecules on {111} terraces, we conclude that the bulk of insertion takes place in massive defect grain boundaries between {111} terraces. Unfortunately, STM images are inherently of poor quality in these disordered regions. For surfaces with greater order, we have shown how insertion can be controlled by controlling the type, density and distribution of film defects.[8,56]

3.5. Comparisons of Scanning Tunneling microscope Images of Different Oligomers: Assignment of Topographic and Electronic Contributions. In this study and the previous one,[5] we have obtained electron-tunneling images of short alkanethiolate SAMs with inserted conjugated molecules containing two, three, and six benzene rings separated by one, two, and five ethynylene links, respectively (Table 1). For purposes
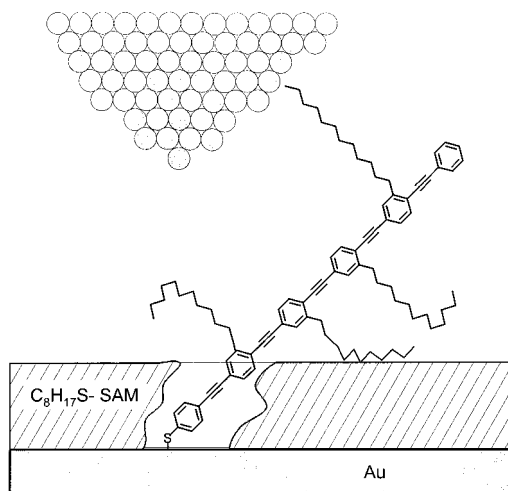
Spectroscopic Characterization of Mixed Surface Assemblies

J. Phys. Chem. B, Vol. 104, No. 20, 2000 **4891**

Figure 14. A schematic illustrating one possible origin of a current spike as the STM tip attempts to maintain constant current in the vicinity of a **3** molecule. While it is not known exactly what the dynamics of the tip−molecule system are during passage of the tip across the surface, one possibility, among many, is a voltage-induced change in the chain conformation, as shown in the figure. The different exponential tunneling probability through a chain compared to vacuum (see ref 9) consequently would lead to a nonlinear change in the tunneling current as the tip−molecule-distance changes.

TABLE 5: Summary of Δh_{model} and Δh_{STM} Values[a] for Selected Combinations of Inserted Linear Conjugated Molecules and Host SAMs

inserted molecule	SAM	Δh_{model}, Å[b]	Δh_{STM}, Å
1	A12	+2.8	5 ± 1[c]
2	A8	+2.1	3.3 ± 0.3
2	A10	+0.1	2.5 ± 0.3
2	A12	−2.3	2.3 ± 0.3
2	A14	−4.4	2.3 ± 0.3
3	A8	+25.1	9 ± 1[d]

[a] The Δh quantities are defined in the text. [b] Estimated from molecular models with the assumption that the inserted molecules are tilted $\sim$30° from the surface normal. [c] Data taken from ref 5. [d] Not including 20−40 Å current spikes arising during the scans. See text for details.

of comparison, we have summarized in Table 5 the Δh_{model} and Δh_{STM} values obtained in these studies.

We do not expect the physical height differences (Δh_{model}) between the inserted molecules (**1**, **2**, **3**) and the host matrix alkanethiolates (**A8**, **A10**, **A12**, **A14**) to be related in a simple fashion to the STM feature differences (Δh_{STM}). While Δh_{model} is purely a structural quantity, Δh_{STM} also depends on electronic properties. In recent work we have imaged highly ordered, mixed alkanethiolate lattices with contiguous domains of different length chains. These results show that differences between Δh_{model} and Δh_{STM} can be understood quantitatively in terms of the differences in the transconductances of the individual chains and the associated tunneling gap for images where the tip is positioned outside the films.[9] Moreover, the electron-transfer decay probability per unit chain length β[57] was shown to have the same value of $\sim$3 Å per $[-CH_2-CH_2-]$ unit at a 1 V bias as has been reported for electron tunneling through alkyl chains in a variety of electrochemical systems.[9] These data demonstrate that the STM tunneling through alkyl chains involves a universal molecular transconductance process. We expect this mechanism to hold for other classes of molecules, such as the conjugated oligomers in this study. However, quantitative comparisons require that the molecules be in identical conformations and environments.[9] These conditions are *not* met for typical cases where the guest molecules

insert in an uncontrolled fashion into a variety of film defects. We recently have begun work on creating films with many identical two-dimensional matrix isolation sites where molecules can be inserted in more uniform ways for study.[58]

4. Conclusions and Future Work

This study shows that phenylethynyl oligomers, with a range of lengths and side or terminal groups, can be inserted into defect sites in self-assembled alkanethiol monolayers of various thicknesses. The nitro-terminated molecule **2**, with a length within the range of those of the host alkanethiolate molecules, assumes a composition-independent orientation in the host films with a tilt of $\sim$37($\pm$15)° of the long molecular axis, similar to the tilt of the host alkanethiolate chains ($\sim$30°). In contrast, the tilt of the long inserted oligomer **3** ($\sim$40 Å) in the relatively short host SAMs decreases with decreasing oligomer fraction and approaches a value similar to that of inserted **2**. From comparisons of experimental and theoretically predicted (DFT) shifts of the IRS peak positions of the vibrational modes of **2**, we deduce that when the extension of **2** above the substrate is shorter than the host film thickness, the alkyl chains are densely packed around the guest molecules. Such precise geometry definitions are used to help interpret the electronic and topographic contributions in the STM images.

Inserted **2** and **3** oligomer molecules are distinguished from the surrounding matrix by their STM feature tip−sample distance profiles, as measured in the constant current mode. In all images, both oligomers appear as protrusions from the host SAMs, even in the case of a tetradecanethiolate host with the relatively shorter **2** molecules inserted. When inserted into host octanethiolate SAMs, **2** appears as a $\sim$2.5 Å protrusion, whereas the longer **3** appears as a $\sim$9 Å protrusion. Additionally, the oligomer **3** yields current spikes in the images, due to the difficulty in maintaining stable tip-**3**−Au junction currents. Overall, these results show, as expected from the fully conjugated nature of the oligomers, that the inserted molecules are more conductive than the alkanethiolate molecules. Experiments to quantify the transconductance of these isolated conjugated molecules are underway.[58b]

The greater conductivity of these phenylethynyl oligomers presents opportunities for the development and testing of molecular-scale electronics. In addition, the method for comparing the conductivity of single molecules which is presented here may prove useful in the design and analysis of other types of backbone structures for specific molecular electronic components.

References and Notes

(1) (a) Metzger, R. M.; Panetta, C. A. *New J. Chem.* **1991**, *15*, 209. (b) Gomez-Lopez, M.; Preece, J. A.; Stoddart, J. F. *Nanotechnology* **1996**, *7*, 183.
(2) Freitas, R. A., Jr. *Artif. Cells, Blood Substitutes, Immobilization Biotechnol.* **1998**, 26, 411.
(3) (a) Aviram, A.; Ratner, M. A. *Chem. Phys. Lett.* **1974**, *29*, 277. (b) Goldhaber-Gordon, D.; Montemerlo, M. S.; Love, J. C.; Opiteck, G. J.;

4892 *J. Phys. Chem. B, Vol. 104, No. 20, 2000*

Dunbar et al.

Ellenbogen, J. C. *Proc. IEEE* **1997**, *85*, 521. (c) Wada, Y. *Surf. Sci.* **1997**, *386*, 265. (c) Roth, S.; Burghard, M.; Leising, G. *Curr. Opin. Solid State Mater. Sci.* **1998**, *3*, 209. (d) Joachim, C.; Gimzewski, J. K. *Proc. IEEE* **1998**, *86*, 184. (e) Sato, T.; Ahmed, H.; Brown, D.; Johnson, B. F. G. *J. Appl. Phys.* **1997**, *82*, 696.

(4) Allara, D. L.; Dunbar, T. D.; Weiss, P. S.; Bumm, L. A.; Cygan, M. T.; Tour, J. M.; Reinerth, W. A.; Yao, Y.; Kozaki, M.; Jones, L., II, *Ann. N. Y. Acad. Sci.* **1998**, *852*, 349.

(5) Cygan, M. T.; Dunbar, T. D.; Arnold, J. J.; Bumm, L. A.; Shedlock, N. F.; Burgin, T. P.; Jones, L., II; Allara, D. L.; Tour, J. M.; Weiss, P. S. *J. Am. Chem. Soc.* **1998**, *120*, 2721.

(6) Bumm, L. A.; Arnold, J. J.; Cygan, M. T.; Dunbar, T. D.; Burgin, T. P.; Jones, L., II; Allara, D. L.;. Tour. J. M.; Weiss, P. S. *Science* **1996**, *271*, 1705.

(7) (a) Eigler, D. M.; Weiss, P. S.; Schweizer, E. K.; Lang, N. D. *Phys. Rev. Lett.* **1991**, *66*, 1189. (b) Weiss, P. S.; Eigler, D. M. *Phys. Rev. Lett.* **1993**, *71*, 3139. (c) Salmeron, M.; Neubauer, G.; Folch, A.; Tomitori, M.; Ogletree, D. F.; Sautet, P. *Langmuir* **1993**, *9*, 3600. (d) Weiss, P. S. *Trends Anal. Chem.* **1994**, *13*, 61.

(8) Bumm, L. A.; Arnold, J. J.; Charles, L. F.; Dunbar, T. D.; Allara, D. L.; Weiss, P. S., *J. Am. Chem. Soc.* **1999**, *121*, 8017.

(9) Bumm, L. A.; Arnold, J. J.; Dunbar, T. D.; Allara, D. L.; Weiss, P. S. *J. Phys. Chem. B* **1999**, *103*, 8122.

(10) The chemical structure of **1** was incorrectly given in refs 5 and 6. The location of the ethyl group is correctly shown in Table 1 of this article.

(11) Chen, J.; Reed, M. A.; Rawlett, A. M.; Tour, J. M. *Science* **1999**, *286*, 1550.

(12) (a) Pearson, D. L.; Tour, J. T. *J. Org. Chem.* **1997**, *62*, 1376. (b) Jones, L., II; Schumm, J. S.; Tour, J. M. *J. Org. Chem.* **1997**, *62*, 1388.

(13) Tour, J. M.; Jones, L., II; Pearson, D. L.; Lamba, J. J. S.; Burgin, T. P.; Whitesides, G. M.; Allara, D. L.; Parikh, A. N.; Atre, S. V. *J. Am. Chem. Soc.* **1995**, *117*, 9529.

(14) The Au films on mica substrates consisted of tabular grains with large (micrometer scale) Au{111} terraces which were ideal for STM studies. The poor end-to-end flatness of the thin mica substrates preclude their efficient use for reflection IR. In contrast, the Au/Cr/SiO₂/Si films exhibited small (~10−50 nm) Au{111} terraces with ~20−30% of grain boundary regions which made STM measurements difficult but the excellent flatness make these samples ideally suited for IRS (see ref 5 and Nuzzo, R. G.; Fusco, F. A.; Allara, D. L. *J. Am. Chem. Soc.* **1987**, *109*, 2358). A variety of previous work shows that despite these morphology differences between the two types of Au samples the character of the alkanethiolate SAMs is highly similar. For example, infrared spectral features for ambient temperature films are virtually identical for good quality polycrystalline Au (see ref 15) and {111} single-crystal surfaces (e.g., Nuzzo, R. G.; Korenic, E. M.; Dubois, L. H. *J. Chem. Phys.* **1990**, *93*, 767−773), thus showing a similar high degree of conformational order. Further, IR (ref 15) data on polycrystalline Au, X-ray scattering data on {111} single crystals (see, e.g., Fenter, P.; Eberhardt, A.; Eisenberger, P. *Science* **1994**, *266*, 1216−1218) and theoretical estimates (e.g., Gerdy, J. J.; Goddard, W. A. *J. Am. Chem. Soc.* **1996**, *118*, 3233−3236) all agree on a uniform chain tilt angle value of 28° within a ±2° range. Finally, electrochemical studies show that alkanethiolate SAMs on polycrystalline Au surfaces have low defect contents in terms of the ability to effectively block Faradaic current flow to the electrode (e.g., Porter, M. D.; Bright, T. B.; Allara, D. L.; Chidsey, C. E. D. *J. Am. Chem. Soc.* **1987**, *109*, 3359). These studies together imply that the alkanethiolate chains that form in Au grain boundary regions retain high packing densities and a high degree of conformational ordering relative to the structure on the {111} terraces. Undoubtedly there will be a decay of film translational ordering in the grain boundary regions. Unfortunately, the molecular spacings in these perturbed grain boundary regions cannot be readily characterized by scattering or scanning tip probes.

(15) Laibinis, P. E.; Whitesides, G. M.; Allara, D. L.; Tao, Y.-T.; Parikh, A. N.; Nuzzo, R. G. *J. Am. Chem. Soc.* **1991**, *113*, 7152.

(16) Collins, R. W.; Allara, D. L.; Kim, Y.-T.; Lu, Y.; Shi, J. In *Characterization of Organic Thin Films*; Ulman, A., Ed.; Manning: Greenwich, CT, 1995; pp 35−55.

(17) Shi, J.; Hong, B.; Parikh, A. N.; Collins, R. W.; Allara, D. L. *Chem. Phys. Lett.* **1995**, *246*, 90.

(18) Parikh, A. N.; Allara, D. L. In *Physics of Thin Films Series*; Vedam, K., Ed.; Academic Press: New York, 1994; Vol. 19 (*Optical Characterization of Real Surfaces Films*), pp 279−314.

(19) Ghose, A. K.; Crippen, G. M. *J. Chem. Inf. Comput. Sci.* **1987**, *27*, 21.

(20) Immirzi, A.; Perini, B. *Acta Crystallogr.* **1971**, *A 33*, 216. Because of possible errors due to the small sizes of crystals used in the float method of density determination, the above-referenced density estimation method was used as a check. Calculated densities were within 5% of those measured.

(21) The effective medium approximation is wavelength independent and is applicable to both SWE and IRS calculations. The Maxwell−Garnet approximation used follows our earlier treatment (Tao, Y.-T.; Hietpas, G. D.; Allara, D. L. *J. Am. Chem. Soc.* **1996**, *118*, 6724. Also see: Aspnes, D. E. *Thin Solid Films* **1982**, *89*, 249). Briefly, the effective complex optical function tensor (or scalar) for a heterogeneous film layer is calculated from the equation $\epsilon = \epsilon_a(1 + 2f_b\Omega/(1 - f_b\Omega)$ where, $\epsilon = n^2$, ϵ_a. and ϵ_b are the complex dielectric functions (expressed as scalars or tensors) for medium a containing embedded b, f_b = volume fraction of component b (with $f_a > f_b$) and $\Omega = \epsilon_b - \epsilon_a/\epsilon_b + 2\epsilon_a$.

(22) Parikh, A. N.; Allara, D. L. *J. Chem. Phys.* **1992**, *96*, 927.

(23) For recent examples involving aromatic ring molecules, see: (a) Liedberg, B.; Yang, Z.; Engquist, I.; Wirde, M.; Gelius, U.; Götz, G.; Bäuerle, P.; Rummel, R.-M.; Ziegler, Ch.; Göpel, W. *J. Phys. Chem. B* **1997**, *101*, 5951. (b) Young, J. T.; Boerio, F. J.; Zhang, Z.; Beck, T. L. *Langmuir* **1996**, *12*, 1219.

(24) The prominent thioacetyl modes observed in the starting compounds are 1710 cm⁻¹ (symmetric C=O stretch), 1120 cm⁻¹ (OC−CH₃ stretch), and 956 cm⁻¹ (S−CO stretch).

(25) The humidity of the chamber during imaging was found to be critical in obtaining quality images. At relative humidities above 10%, the monolayers often appeared featureless and streaky. At lower humidities, molecular resolution images were routinely obtained.

(26) Takami, T.; Delamarche, E.; Michel, B.; Gerber, Ch.; Wolf, H.; Ringsdorf, H. *Langmuir* **1995**, *11*, 3876.

(27) (a) Camillone, N., III; Eisenberger, P.; Leung, T. Y. B.; Scoles, G.; Poirier, G. E.; Tarlov, M. J. *J. Chem. Phys.* **1994**, *101*, 11031. (b) Delamarche, E.; Michel, B.; Gerber, Ch.; Anselmetti, D.; Guntherodt, H.-J.; Wolf, H.; Ringsdorf, H. *Langmuir* **1994**, *10*, 2869.

(28) (a) Wong, M. W.; Frisch, M. J.; Wiberg, K. B. *J. Am. Chem. Soc.* **1991**, *113*, 4776. (b) Wong, M. W.; Wiberg, K. B. *J. Chem. Phys.* **1991**, *95*, 8991. (c) Wong, M. W.; Wiberg, K. B.; Frisch, M. J. *J. Am. Chem. Soc.* **1992**, *114*, 523. (d) Wong, M. W.; Wiberg, K. B.; Frisch, M. J. *J. Am. Chem. Soc.* **1992**, *114*, 1645.

(29) Frisch, M. J.; Trucks, G. W.; Schlegel, H. B.; Gill, P. M. W.; Johnson, B. G.; Robb, M. A.; Cheeseman, J. R.; Keith, T.; Petersson, G. A.; Montgomery, J. A.; Raghavachari, K.; Al-Laham, M. A.; Zakrzewski, V. G.; Ortiz, J. V.; Foresman, J. B.; Cioslowski, J.; Stefanov, B. B.; Nanayakkara, A.; Challacombe, M.; Peng, C. Y.; Ayala, P. Y.; Chen, W.; Wong, M. W.; Andres, J. L.; Replogle, E. S.; Gomperts, R.; Martin, R. L.; Fox, D. J.; Binkley, J. S.; Defrees, D. J.; Baker, J.; Stewart, J. P.; Head-Gordon, M.; Gonzalez, C.; Pople, J. A. *Gaussian 94,* Revision E.2; Gaussian, Inc.: Pittsburgh, 1994.

(30) (a) Rauhut, G.; Pulay, P. *J. Phys. Chem.* **1995**, *99*, 3093. (b) DegliEsposti, A.; Zerbetto, F. *J. Phys. Chem. A* **1997**, *101*, 7283.

(31) Ramondo, R. *Can. J. Chem.* **1992**, *70*, 314.

(32) Laposa, J. D. *Spectrochim. Acta* **1979**, *35 A*, 65.

(33) Lide, D. R., Ed. *CRC Handbook of Chemistry and Physics,* CRC Press: Boca Raton, FL, 1990.

(34) The presence of negative frequencies reveals that the structure is at a saddle point on the geometric potential energy surface.

(35) Varsyanyi, G. *Assignments for Vibrational Spectra of Seven Hundred Benzene Derivatives*; Wiley: New York, 1974; Vol. 1.

(36) Since $\lambda_{max} = 362$ nm for the similar compound (Matsuzawa, M.; Dixon, D. A. *J. Phys. Chem.* **1992**, *96*, 6232), $k(632.8$ nm$) \sim 0$ so $\hat{n}(632.8$ nm$) \sim n$. Application of an isotropic film model of a pure **2** monolayer with $n = 1.64$ consistently results in thickness values of $d = 17.8$ Å, greater than the physical length of **2** (13.5 Å, Table 1). All interpretations of the IRS spectrum of **2** on gold (Figure 2), however, show that the adsorbate molecules are tilted from the surface normal. Consequently, anisotropic film models are required for analyzing the ellipsometry data. The anisotropic behavior can be estimated from the work of Matsuzawa and Dixon (ref. above). These authors calculated polarizabilities for nitrotolane methyl sulfide of $\alpha_{xx} = 21.94$ Å³, $\alpha_{yy} = 6.32$ Å³, and $\alpha_{zz} = 54.37$ Å³, and noted that the experimental polarizabilities were routinely 0.75 times that of experiment. Using this correction factor our case and setting $\alpha'_{xx} = \alpha'_{yy} = 1/2(\alpha'_{xx} + \alpha'_{yy})$, yields $\alpha'_{xx} = \alpha'_{yy} = 18.8$ Å³, and $\alpha'_{zz} = 72.5$ Å³. Applying these values to den Engelsen's cylindrical model (*Surf. Sci.* **1976**, *56*, 272) with a length and cross section of 15 and 24.5 Å², respectively, results in $(n_{zz} - n_{xx}) = \Delta n_{xz} \sim 0.6$, with $n_{xx} = n_{yy}$. Minor deviations from these values (±1 Å length and ±4 Å² area) yield Δn values for molecule **2** of between 0.55 and 0.63. Using an anisotropic model with $\Delta n_{xz} \sim 0.6$ and a variety of long molecular axis tilts still leads to thickness values greater than the molecular length. For example, tilts of 0 and 37° give $d = 15.8$ and 16.4 Å, respectively. Inclusion of a small imaginary contribution ($k_{avg} = 0.1$) with the maximum possible anisotropy ($k_{zz} = 0.3$, $k_{xx} = k_{yy} = 0$) gives $d = 16.2$ Å. This leaves a discrepancy with the physical length of the molecule of $16.2 - 13.5 = 3.7$ Å. The discrepancy could be partially resolved by larger values of n. For denser packing in the monolayer compared to the bulk, $n_{film} > n_{bulk}$. For example, a film density of 1.5 g cm⁻³ would result in $n_{avg} = 1.8$. It is also possible that the known Au to S electron transfer (ref 17) in alkanethiolate monolayers could be enhanced by the electronegative NO₂ group. This effect could change the interface layer optical constant (see ref 17) and/or increase the refractive index anisotropy of **2** by increasing the polarizability along the long molecular axis. The interface layer is neglected in our models because of the difficulty of determining perturbations for SAMs without independently fixed structures. With regard to the second effect, using $n_{avg} = 1.8$, $\Delta n_{xz} \sim 1.0$, and a small anisotropic k ($k_{zz} = 0.3$, k_{xx}

Spectroscopic Characterization of Mixed Surface Assemblies

J. Phys. Chem. B, Vol. 104, No. 20, 2000 **4893**

$= k_{yy} = 0$) yields d $\sim$14.6 Å. This leaves a discrepancy of 14.6$-$13.5 = 1.6. Further changes in any of these parameters to give thickness values approaching the limit of the molecular length (13.5 Å) become physically unrealistic.

(37) These shifts arise from intrinsic perturbations of the bonding potentials in the two molecular environments. Accompanying perturbations of the charge flow dynamics, and thus the intrinsic mode intensities, also can be expected.

(38) (a) Collard, D. M.; Fox, M. A. *Langmuir* **1991**, *7*, 1192. (b) Schlenoff, J. B.; Li, M.; Ly, H. *J. Am. Chem. Soc.* **1995**, *117*, 12528. (c) Biebuyck, H. A.; Whitesides, G. M. *Langmuir* **1993**, *9*, 1766.

(39) Porter, M. D.; Bright, T. B.; Allara, D. L.; Chidsey, C. E. D. *J. Am. Chem. Soc.* **1987**, *109*, 3359.

(40) Schönenberger, C.; Jorritsma, J.; Sondag-Huethorst, J. A. M.; Fokkink, L. G. J. *J. Phys. Chem.* **1995**, *99*, 3259.

(41) Poirier, G. E.; Tarlov, M. J. *Langmuir* **1994**, *10*, 2853.

(42) Given the dense packing of the chains on the terraces, the exchange mechanism at the terraces could involve a preliminary desorption of an adsorbate chain followed by backfilling of the transient hole. The latter could occur by transport of a solute molecule or by migration of the hole via adsorbate hopping to a SAM defect region where solute insertion could occur (see: Stranick, S. J.; Parikh, A. N.; Tao, Y.-T.; Allara, D. L.; Weiss, P. S. *J. Phys. Chem.* **1994**, *98*, 7636). Studies to determine this mechanism are underway in our laboratories.

(43) The height differences were determined in the following manner. The S$-$Au bond distances of alkanethiolate and arylthiolate were assumed to be equal. The lengths of each type of molecule were specified as the S to end atom distance, S to terminal CH_3 hydrogen of an all-trans alkanethiolate and S to terminal O of **2a**, and were determined from molecular mechanics modeling (Hyperchem). Each length was then multiplied by cos 30° to account for the tilt.

(44) Herzberg, G. *Infrared and Raman Spectra of Polyatomic Molecules*; Van Nostrand Reinhold: New York, 1945; pp 534$-$537.

(45) Pouchert, C. J., Ed. *The Aldrich Library of FT-IR Spectra*; Aldrich Chemical Co.: Milwaukee, WI, 1985 (Vol. 1), 1989 (Vol. 3).

(46) Weiss, P. S.; Bumm, L. A.; Dunbar, T. D.; Burgin, T. P.; Tour, J. M.; Allara, D. L. *Ann. N. Y. Acad. Sci.* **1998**, *852*, 145.

(47) The errors in θ and ψ come from fitting simulations to films of 21 and 25 Å (the two limits of thickness given an uncertainty of $\pm$2 Å). This uncertainty in thickness also roughly covers errors arising from neglecting refractive index anisotropy in the ellipsometric thickness calculation. Repeating simulations for the high and low limits on thickness led to high and low tilt angles and low and high twist angles.

(48) (a) Snyder, R. G.; Strauss, H. L.; Elliger, C. A. *J. Phys. Chem.* **1982**, *86*, 5145. (b) MacPhail, R. A.; Strauss, H. L.; Snyder, R. G.; Elliger, C. A. *J. Phys. Chem.* **1984**, *88*, 334.

(49) Snyder, R. G.; Maroncelli, M.; Strauss, H. L.; Hallmark, V. M. *J. Phys. Chem.* **1986**, *90*, 5623

(50) The most accurate model would consist of a distribution of isolated **3** molecules and bundles of **3** molecules, inserted at various defect sites in the **A8** SAM, as observed by STM imaging (see section 3.3.2). Application of this model would require accurate knowledge of the optical response (optical or dielectric functions) of (1) *isolated* **3** molecules partially immersed in a vacuum (or a gas-phase) and partially in a hydrocarbon medium and (2) the pure solid phase of **3**. Since data for the two states of case 1 would be extremely difficult to obtain, more approximate models were chosen based on case 2 in which the polycrystalline form of **3b** was used as a reference state for the inserted molecules.

(51) We estimate that errors in using the isotropic approximation are less than the experimental SWE measurement errors. While one expects some degree of anisotropy for the long conjugated aromatic portion of molecule **3**, the alkyl chain portion, which comprises over 50% of the atoms in the molecule, is highly disordered (see discussion of the high frequency IRS data) and thus essentially isotropic. The net result is that the entire molecule exhibits only weak optical anisotropy.

(52) In practice, for each measured Δ value a plot of f_3 vs d_{film}, a hyperbola-like curve, was generated. Once a value of θ was estimated from the IRS mode intensity ratio procedure, a value of d_{film} was estimated from $d_{film} = d_3 \cos \theta$, where, $d_3 = 40.2$ Å, the length of the **3** molecule (Table 1). Using the f_3 vs d_{film} curve, a new value of f_3 was determined for input into a new IRS simulation.

(53) The **A8** parent molecules are liquids at ambient temperatures so no convenient polycrystalline reference state is available for spectral measurements. Instead, an optical function spectrum [$\hat{n}_{SAM}^{A8}(\tilde{v})$] was derived directly from the spectrum of the pure **A8** SAM using a simple 3-medium model (Au/film/air) in which the film was treated as isotropic. The pseudo optical function $\hat{n}_{SAM}^{A8}(\tilde{v})$ will generate back the exact pure **A8** SAM spectrum and is essentially a simple way to approximate the optical effects of the presence of a partial coverage **A8** SAM in a composite layer of thickness $d_2 = d_{A8}$ with a coverage of $(1 - f_3)$.

(54) Using the bond additivity model of Wetter et al. (Wetterer, S. M.; Lavrich, D. J.; Cummings, T.; Bernasek, S. L.; Scoles, G. *J. Phys. Chem. B* **1998**, *102*, 9266) we estimate $\sim$740 kJ mol^{-1} as the physisorption energy of **3** on Au{111} for a flat configuration. In comparison, the predicted physisorption energy for benzene is 57.9 kJ mol^{-1}.

(55) Poirier, G. E.; Pylant, E. D. *Science* **1996**, *272*, 1145.

(56) Weck, M.; Jackiw, J. J.; Rossi, R. R.; Weiss, P. S.; Grubbs, R. H. *J. Am. Chem. Soc.* **1999**, *121*, 4088.

(57) The tunneling current through a medium is defined by $j \propto e^{-\beta l}$, where j = tunneling current, l = tip to substrate distance through the medium, and β = the decay constant associated with the medium.

(58) (a) Charles, L. F. M.S. Thesis, The Pennsylvania State University, University Park, PA. (b) Charles, L. F.; Weiss, P. S. In preparation.